TECHNICAL MEMORANDUM

412

Variational retrieval of temperature and humidity profiles using rain rates versus microwave brightness temperatures

Emmanuel Moreau, Philippe Lopez,
Peter Bauer, Adrian M. Tompkins,
Marta Janisková and Frédéric Chevallier

Research Department

Submitted to Q. J. Roy. Meteor. Soc.

July 2003

European Centre for Medium-Range Weather Forecasts
Europäisches Zentrum für mittelfristige Wettervorhersage
Centre européen pour les prévisions météorologiques à moyen terme

For additional copies please contact

The Library
ECMWF
Shinfield Park
Reading
RG2 9AX
library@ecmwf.int

Series: ECMWF Technical Memoranda

A full list of ECMWF Publications can be found on our web site under:
http://www.ecmwf.int/publications/

Abstract

This paper assesses the performance of two different approaches for the retrieval of temperature and humidity profiles from the satellite passive microwave measurements of the Tropical Rainfall Measuring Mission (TRMM) and of the Special Sensor Microwave Imager in rainy areas. Both methods are based on a one-dimensional variational retrieval (1D-Var) approach. The input to the first one is rainfall rates estimated by a standard retrieval algorithm from the raw brightness temperatures. In the second technique, 1D-Var directly uses the brightness temperatures. The retrieval experiments utilize new simplified physical parameterizations of convection and large-scale condensation specially designed for variational assimilation as well as a microwave radiative transfer model.

Several tropical and mid-latitude meteorological situations are studied. In all cases, it is found that both 1D-Var approaches are able to converge satisfactorily and produce consistent temperature and specific humidity increments. However, the convergence of 1D-Var retrievals on surface rainfall rates and to a lesser extent of 1D-Var retrievals on brightness temperatures is reduced when precipitation in the background is produced through convection and not by large-scale processes. The results of the two 1D-Var methods are then compared in brightness temperature and rainfall rate space and are validated against independent observations from the precipitation radar on-board TRMM. Finally, the sensitivity of the 1D-Var retrievals to the specification of observation error statistics is studied.

1 Introduction

The assimilation of observations related to clouds and precipitation has become an important issue for a number of operational weather forecasting centres, including the European Centre for Medium-range Weather Forecasts (ECMWF). In particular, the representation of the hydrological cycle in numerical weather prediction models will be one of the major challenges in the next few years. Observations are already available from the Tropical Rainfall Measuring Mission (TRMM) since 1997, from the satellites of the US Defense Meteorological Satellite Program (DMSP) since 1987, and from the Aqua mission since May 2002. This study utilizes data from the TRMM Microwave Imager (TMI) and from the DMSP Special Sensor Microwave/Imager (SSM/I). In the coming years, an increasing amount of observations related to clouds and precipitation is likely to become available from lidars, radars and imagers installed on board satellite missions such as the Special Sensor Microwave Imager/Sounder SSMIS (2003), CloudSat (2004), the Cloud-Aerosol Lidar and Infrared Pathfinder Satellite Observations mission (CALIPSO; 2004), the Global Precipitation Mission (GPM; 2008) and the Earth Cloud Aerosol Radiation Experiment (EarthCARE; 2008). Maximizing the benefits from this huge source of data will require the development of assimilation procedures capable of efficiently converting the information on clouds and precipitation into realistic increments applicable to the forecast model's variables (temperature, humidity, wind, and possibly clouds and precipitation themselves).

Marécal and Mahfouf (2000) developed a unidimensional variational (1D-Var) method for correcting individual profiles of the ECMWF model's control variables in order to decrease the discrepancies that often exist between the simulated surface rainfall rates (RR) and corresponding retrievals obtained from TMI or SSM/I microwave brightness temperatures (TB). Marécal and Mahfouf (2002) also demonstrated that an indirect "1D-Var + 4D-Var" assimilation of TMI derived rainfall rates could improve the quality of humidity, temperature and wind forecasts in the Tropics. In their approach, the background-observation departures on surface rainfall rates are first converted into total column water vapour (TCWV) increments as an output from 1D-Var retrievals. The corresponding TCWV pseudo-observations are then assimilated in the 4D-Var system. They also showed that this indirect method is more robust than a direct 4D-Var assimilation of the TMI rainfall rates, because of some inconsistencies between the inner and outer loops of the ECMWF 4D-Var assimilation system (Courtier *et al.* (1994)). The "1D-Var + 4D-Var" technique therefore seems more appropriate to assimilate such data until these inconsistencies are resolved.

Instead of performing the 1D-Var retrievals on surface rainfall rates that are derived from multi-channel microwave brightness temperatures through various algorithms, the 1D-Var calculations could directly deal with the TBs. This would homogenize the approach and could even provide more accurate retrievals, since the sensitivities of TBs not only to rain, but also to cloud water and water vapour could be exploited (Moreau *al.* 2003). This study explores this new method and compares its performance with that of the existing 1D-Var retrieval applied to derived rainfall rates.

The plan of the paper is as follows. Section 2 introduces the 1D-Var technique used in this paper. This includes a description of two new parameterizations of moist processes that were specially designed for assimilation in order to make a compromise between physical realism and linear behaviour. The microwave radiative transfer model used in the 1D-Var computations is also briefly presented. Section 3 deals with the experimental set-up, which includes the description of the cases studied and of the observational and model datasets (including the specification of error statistics). The main results from the 1D-Var experiments are then detailed in section 4. A discussion on the comparison of 1D-Var on surface rainfall rates with 1D-Var on TBs as well as a validation of the 1D-Var outputs against independent satellite data are proposed in section 5. This section also presents a study of the sensitivity of the 1D-Var retrievals to the specification of the observation error statistics.

2 The 1D-Var retrieval method

2.1 General description

The objective of 1D-Var is to find an optimal model state that minimizes in a least-square sense the distance between a selected output quantity of the model and its observed equivalent, given a background constraint. In the present study, two control variables are considered in the model: temperature and specific humidity. They are given in the form of individual vertical profiles at a given time. The selected output quantity to be optimized is either the surface rainfall rate (as in Marécal and Mahfouf 2000) or the multi-channel microwave brightness temperatures. The two corresponding 1D-Var retrieval methods will be hereafter referred to as 1D/RR and 1D/TB, respectively. Surface rainfall rate is an output from the model's convection and large-scale condensation parameterizations and can be derived from observed microwave brightness temperatures via a retrieval algorithm. On the other hand, brightness temperatures can be simulated by applying the parameterizations of moist processes to the model's control variables followed by the application of a microwave radiative transfer model (RTM). The main inputs to the latter model are precipitation content, cloud water content, cloud cover, specific humidity, air and sea-surface temperatures and surface wind speed. In the present study, the 1D-Var method searches for the model's state vector $\mathbf{x}$ that minimizes the following functional:

$$J(\mathbf{x}) = \frac{1}{2}(\mathbf{x}-\mathbf{x_b})^T\mathbf{B}^{-1}(\mathbf{x}-\mathbf{x_b}) + \frac{1}{2}(H(\mathbf{x})-\mathbf{y}_o)^T\mathbf{R}^{-1}(H(\mathbf{x})-\mathbf{y}_o) \quad (1)$$

where $\mathbf{x}_b$ is the background model state (*i.e.* the model's control vector to be corrected), and $H(\mathbf{x})$ is the nonlinear observation operator that converts the model's variables into either surface rainfall rates or microwave brightness temperatures. $\mathbf{y}_o$ denotes the corresponding observed quantity and $\mathbf{R}$ is the error covariance matrix of the observations, which includes the instrumental errors and the errors of H. Matrix $\mathbf{B}$ contains the background error covariances for the model's control variables (temperature and specific humidity). The result of the 1D-Var retrieval is therefore a combination of the background and of the observation, weighted by the inverse of their respective error statistics.

The minimization of the functional is performed using the quasi-Newton descent algorithm (M1QN3) developed by Gilbert and Lemaréchal (1989). It requires the calculation of the gradient of the functional defined in

Eq. (1) which writes

$$\nabla J(\mathbf{x}) = \mathbf{B}^{-1}(\mathbf{x} - \mathbf{x_b}) + \mathbf{H}^T\mathbf{R}^{-1}(H(\mathbf{x}) - \mathbf{y}_o) \tag{2}$$

where $\mathbf{H}^T$ is the transpose (or adjoint) of the Jacobian matrix of the nonlinear observation operator, H. In this study, H consists of new simplified parameterizations of convection and large-scale condensation that are described in the next subsections. In the case of 1D/TB, H also includes the RTM designed by Bauer (2002) and Moreau *et al.* (2002) that takes into account the scattering of microwave radiation in precipitating clouds.

2.2 Moist physics and the radiative transfer model

2.2.1 Convection

Previous studies advocated an improvement of the linearized version of ECMWF's parameterizations of moist processes, especially convection, to be used in the full 4D-Var and in the simpler 1D-Var algorithm developed by Marécal and Mahfouf (2000). A modified version of the operational convection scheme was therefore developed for the future variational assimilation of clouds and precipitation observations. The modified mass-flux convection scheme was designed such as to retain some basic similarities with the original mass-flux scheme from Tiedtke (1989) and at the same time to remove the high degree of complexity of the latter, which is a source of nonlinearities. Its detailed description and evaluation are presented in Lopez and Moreau (2003) but its main features will be summarized here.

All types of convection (shallow, mid-level, and deep) are treated in a similar way. In particular, the closure assumption that relates the model control variables to the subgrid-scale cloud base mass flux is expressed through a single formulation based on the release of Convective Available Potential Energy (CAPE) in time. In contrast with the operational scheme, the equations that describe the vertical evolution of the updraught mass flux, M_u, and of the updraught thermodynamic variables, Φ_u, are uncoupled:

$$\frac{\partial M_u}{\partial z} = -(\varepsilon - \delta)M_u \tag{3}$$

$$\frac{\partial \Phi_u}{\partial z} = -\varepsilon(\Phi_u - \overline{\Phi}) \tag{4}$$

where $\overline{\Phi}$ denotes field values in the environment, and ε and δ are the fractional entrainment and detrainment rates, respectively. This uncoupling allows the removal of the iterative calculations involved in the operational code for updating the cloud base mass flux, thereby leading to an easier development of the adjoint. The impact of this modification on the forecast is marginal.

Convection is assumed to be activated only if the bulk convective updraught vertical velocity remains positive at cloud base. The updraught is assumed to originate from the surface only if its initial vertical velocity, as calculated from the surface heat fluxes using Holtslag and Moeng (1991), is positive. The departures of the updraught from the environment are also assumed to be dependent on the surface heat fluxes. If convection cannot be initiated from the surface, the convective ascent may originate from higher levels provided relative humidity exceeds 80%. In this case, the initial vertical velocity of the bulk updraught is set equal to 1 m s^{-1}. Regardless of whether the updraught originates from the surface or higher up, the vertical evolution of its kinetic energy is computed following Simpson and Wiggert (1969).

Based on Siebesma and Jakob (personal communication), ε is parameterized as $c_\varepsilon/(z - z_{st}) + 10^{-5}$ where c_ε=0.5 and z_{st} is the starting altitude of the updraught, while $\delta = \varepsilon$, except close to cloud top where a constant organized detrainment rate is added ($\delta = \varepsilon + 2 \times 10^{-4}$).

Simplified calculations of downdraughts and convective momentum transport based on the operational scheme (Tiedtke 1989) are also included in the new parameterization. More importantly, the precipitation formation rate is made proportional to the updraught cloud water content as in Tiedtke (1989).

Reasonably well-behaved physical parameterizations in terms of linearity are necessary to ensure the convergence of the 1D-Var retrievals. Therefore, the linear behaviour of the modified convection scheme compared to the operational one has also been assessed through the calculations of nonlinear residuals. For a given nonlinear operator M and its tangent-linear version $\mathbf{M}^{l}$, the nonlinear residuals are defined as

$$RES_{NL} = M(\mathbf{x} + \lambda\,\delta\mathbf{x}) - M(\mathbf{x}) - \mathbf{M}^{l}[\mathbf{x}]\lambda\,\delta\mathbf{x} \tag{5}$$

where $\mathbf{x}$ denotes the input temperature and specific humidity in the present case. The residuals have been computed for the convective tendencies $\partial T/\partial t$ and $\partial q/\partial t$ that are produced by the convective parameterization M. The calculations of Eq. (5) have been repeated for values of the scaling factor λ ranging from 10^{-5} to 1, and from -10^{-5} to -1. The reference vector of perturbations $\delta\mathbf{x}$ was set equal to typical values of the standard deviation of the background model errors. An example of vertical profiles of such errors is shown in Fig. 1. Figure 2 shows nonlinear residuals, averaged over 100 convective profiles, that are obtained when specific humidity perturbations of varying size are applied at the lowest model level. Results are shown for this level because input perturbations imposed there result in maximum changes in the profiles of convective tendencies. The field actually plotted in Fig. 2 is $\log_{10}(RES_{NL}/RES_{NL}^{max})$ where RES_{NL}^{max} denotes the maximum value of the residual for a given plot and for both the modified and the operational schemes. This normalization permits the comparison of the residuals obtained with the two parameterizations and the smaller the values of the plotted field, the more valid the linear assumption. Figure 2 demonstrates that the nonlinear residuals are almost systematically one order of magnitude smaller with the new scheme than with the operational one. Asymmetries about the y-axis result from the fact that large negative moisture perturbations at the surface turn off convection, thereby leading to a less linear behaviour of the scheme. Note that similar conclusions can be drawn when input perturbations are imposed on temperature instead of specific humidity (Lopez and Moreau 2003).

2.2.2 Clouds

Tompkins and Janisková (2003) have recently developed a new statistical diagnostic cloud scheme that is intended to be implemented instead of the simplified parameterization currently used in ECMWF 4D-Var tangent-linear and adjoint calculations (Janisková *et al.* 2002). A uniform Probability Density Function (PDF) was chosen to describe the subgrid scale fluctuations of temperature and total water in order to make adjoint developments easier and to ensure a reasonable degree of consistency with the scheme used in the full operational forecast model (Tiedtke 1993). The width of the PDF is assumed to increase linearly when relative humidity, RH, varies from 100% down to a critical threshold, RH_0, beyond which cloud formation occurs. Both the slope of this linear dependence and RH_0 are functions of the normalized pressure vertical coordinate P/P_{surf}, where P is the pressure on the current level, and P_{surf} is the surface pressure. In particular, RH_0 ranges from 50% in the mid-troposphere to 85% at the surface and at upper levels.

Large-scale cloud cover is expressed as a function of RH and RH_0, while convective cloud cover depends on the diagnostic source term associated with convective detrainment. The new simplified cloud scheme includes a parameterization of precipitation generation inspired from Sundqvist (1989) and an original parameterization of precipitation evaporation based on the subgrid scale variability of total water.

Tompkins and Janisková (2003) show that the linearity of the new simplified cloud scheme is suitable for its use in 1D-Var and 4D-Var.

2.2.3 Microwave Radiative Transfer

For simulating the radiative transfer in clouds and precipitation for large data volumes the fast modelling framework RTTOV (Eyre 1991, Saunders *et al.* 2002) has been chosen. The multiple scattering is simulated applying the δ-Eddington approximation that has proven to provide sufficient accuracy (Kummerow 1993) at microwave frequencies. All hydrometeor types (rain, snow, cloud liquid water and cloud ice) are assumed to be spherical and their optical properties are taken from pre-calculated look-up Mie tables to increase numerical efficiency (Bauer 2002). For the purpose of variational retrievals as well as to increase computational efficiency, the tangent linear and the adjoint versions of the RTM are employed.

3 Experimental set-up

3.1 Meteorological events

Three recent meteorologically interesting events have been identified for running 1D-Var: Two tropical cyclones well sampled by both TMI and the TRMM precipitation radar (PR) and one extra-tropical front with a good observational coverage from SSM/I. These cases were correctly forecast by the ECMWF operational model in terms of location but not with regards to their structure and rain intensity.

The first selected situation features super-typhoon Mitag that developed over the Western Pacific in early March 2002. 1D-Var has been tested at 1200 UTC 5 March 2002, when the super-typhoon reached its maximum intensity just east of the Philippines (estimated mean-sea-level pressure minimum of 930 hPa located at 14.2°N/129.9°E).

The second event is tropical cyclone Zoe that developed over the Western Pacific in the vicinity of the Fiji Islands, between 25 December 2002 and 31 December 2002. 1200 UTC 26 December 2002 was the date selected for running the 1D-Var. At that time, the storm was in its intensification phase and its central pressure minimum of 975 hPa was located at 10.7°S/174.1°E.

The third case is an extra-tropical front that developed over the North Atlantic in January 2002 and which was dominated by large-scale precipitation. The 1D-Var experiment was run on the meteorological situation at 1200 UTC 9 January 2002.

3.2 Observations

For super-typhoon Mitag and tropical cyclone Zoe, TMI data from the two TRMM satellite orbits at 1100 UTC 5 March 2002 and 1400 UTC 26 December 2002 have been used, respectively. In the case of the mid-latitude front, the 1D-Var experiments have been based on SSM/I data at 1130 UTC 9 January 2002.

Various algorithms have been tested for retrieving surface rainfall amounts from the multi-channel microwave brightness temperatures observed by TMI and SSM/I. For TMI data, both the TRMM standard rainfall product 2A12 (Kummerow *et al.* 2001) and the Precipitation radar Adjusted TMI Estimation of Rainfall (PATER; Bauer *et al.* 2001) retrievals have been used. PATER employs independent rainfall estimates from TMI and PR over their common swath to derive a rain-dependent calibration curve. A similar principle is applied here in order to apply PATER to SSM/I data (PATER-SSMI, thereafter) by simulating the SSM/I observations with TMI data, that is by reducing the spatial resolution and selecting the common channels.

TMI surface rainfall rates derived with 2A12 and PATER have been used in the cases of Mitag and Zoe. On the

other hand, PATER-SSM/I, Bauer and Schluessel (1993) and Ferraro (1996) have been utilized on SSM/I TBs in the mid-latitude frontal case. All observed rainfall retrievals have then been averaged onto the Gaussian grid of the ECMWF model that corresponds to a T511 spectral truncation (*i.e.* to a grid point resolution of about 40 km), so that observation and model points are co-located. The standard deviations of the observation errors, σ_{obs}, on the retrieved rainfall rates have been arbitrarily set equal to 50% of the rainfall rate for Bauer-Schluessel and Ferraro. For the 2A12 algorithm, the rainfall-dependent errors derived by L'Ecuyer and Stephens (2002) have been applied. For PATER, the errors have been calculated according to Bauer *et al.* (2002) . Finally, a minimum threshold of 0.05 mm h^{-1} has been assigned to σ_{obs} for all algorithms so as to keep a non-zero observation error at non-rainy points.

When using TMI and SSM/I brightness temperatures directly in the 1D-Var retrieval, the observed value at each model grid point has been set equal to the value at the closest TMI pixel in each microwave channel, in order to avoid interpolation problems. For TBs, σ_{obs} has been set to 3 K (resp. 6 K) for the vertically (resp. horizontally) polarized channels, assuming no error correlations between channels. These σ_{obs} values are supposed to represent the contributions from both the instrumental errors and the errors in the observation operator. The uncertainties in the RTM may arise both from the δ-Eddington approximation (Moreau *et al.* 2002) as well as from the microphysical assumptions, in particular on drop size distributions and on the fall velocity, shape and density of hydrometeors. Larger values of σ_{obs} are specified for the horizontal polarization to account for the higher natural variablility of microwave TBs observed with this polarization.

Ideally, the observation errors in 1D-Var should also include the errors of the forward model, but these errors are currently neglected because they are difficult to estimate, especially for the moist physics parameterizations. The sensitivity of the 1D-Var retrievals to the specification of matrix **R** is assessed in section 5.3.

Finally, it should be mentioned that at the end of the minimization, each 1D-Var retrieval is quality-controlled by rejecting it if the analysis−observation departure exceeds $\pm 3\sigma_{obs}$. In this case, the retrieval is reset to the background.

3.3 Background fields

The model's background fields that enter the 1D-Var have been obtained from three 12-hour T511 integrations of the ECMWF model that were started at 0000 UTC 5 March 2002 for Mitag, at 0000 UTC 26 December 2002 for Zoe and at 0000 UTC 9 January 2002 for the North Atlantic front. The input fields include the vertical profiles of temperature and water vapour, but also some temperature and specific humidity tendencies, the surface heat fluxes and the surface momentum stress that are needed for running the modified convection scheme described in section 2.2.1. For 1D/TB, the use of the RTM requires additional input fields, namely 10 m-wind speed, surface temperature, and 2 m-temperature and humidity. The covariance matrix of background errors **B** is taken from the operational ECMWF 4D-Var system (Rabier *et al.* 1997). Figure 1 shows typical values of the standard deviation of the model background errors on temperature and specific humidity which appear along the leading diagonal of matrix **B**. The assumption is made that the temperature and specific humidity errors are uncorrelated.

4 Results

4.1 Super-typhoon Mitag

4.1.1 1D-Var on TMI surface rainfall retrievals

Figure 3 displays the results for the 1D-Var experiments on super-typhoon Mitag: the model background surface rainfall rates are shown in panel (a). Observed rainfall rates as retrieved with the 2A12 algorithm from the TMI TBs are displayed in panel (b). 1D-Var retrievals of surface rainfall rates are shown in panel (c). Panels (d) and (e) display the same quantities when the PATER algorithm is utilized. All fields are expressed in mm h^{-1}. Although some heavy rain is correctly simulated by the model in the vicinity of the typhoon's core, panel (a) indicates that the background clearly differs from the observations in the western periphery of the storm. Indeed, three regions with heavy precipitation that do not appear in the TMI observations are simulated by the model.

Panels (c) and (e) demonstrate that the 1D-Var procedure is able to correct the initial temperature and specific humidity profiles in such way that the 1D-Var retrieved rainfall gets rather close to the observations. This improvement on the picture of the simulated typhoon results from both the increase and the decrease of precipitation at places where the observed value is higher, respectively lower, than the model's background value. However, it should be emphasized that 1D/RR is efficient only at points where the background precipitation is non-zero. At locations where the initial simulated rainfall rate is zero, the Jacobian matrix H is zero, which implies that the minimization is ineffective. In the present case, 1D/RR performs rather well because the new simplified large-scale condensation scheme produces widespread very light rainfall amounts around the storm, which admits more observations to the retrieval procedure. The production of more widespread precipitation in the tropics compared to the operational scheme, can be partly explained by the revised rainfall evaporation formulation used in the simplified parameterization (Tompkins and Janisková 2003). Earlier 1D-Var tests with a simpler parameterization that generated more confined precipitation led to much less satisfactory retrieved surface rain rates.

The convergence of the minimization is usually satisfactory, except at a few grid points for which the analysed rainfall rates remain far from the observations due to nonlinearities in the observation operator H. One should also note that the observed TMI rainfall rates from PATER are substantially lower than the ones obtained from 2A12. Such a difference was already demonstrated by Marécal *et al.* (2002). Generally, the agreement of the 1D-Var retrieved rainfall rates with the corresponding observed values is better when using PATER retrievals than with 2A12 data, which can be explained by the fact that the background is closer to PATER than to 2A12.

Figure 4 shows the vertical profiles of 1D-Var temperature and specific humidity increments averaged over the geographical domain of Fig. 3, with a distinction between points for which the background rainfall rate is either larger or lower than the value retrieved from TMI. These profiles clearly indicate that the reduction (increase) of the model surface rainfall by the 1D-Var retrieval is achieved through a drying and heating (moistening and cooling) of the troposphere below 300 hPa. This latter result can be readily explained by the fact that these increments are mainly obtained by activating the large-scale condensation scheme and not the convective parameterization. Such behaviour was previously found by Fillion and Mahfouf (2000). A simple conversion of the temperature increments into equivalent increments of saturation specific humidity shows that the 1D-Var corrections on temperature are approximately four times smaller than the corrections on specific humidity at all levels, which confirms the results of Marécal and Mahfouf (2000). However, this conclusion is likely to depend on the type of parameterizations used for describing moist processes.

Since the specific humidity increments largely exceed those of temperature (when converted into saturation

specific humidity equivalents), the global impact of the 1D-Var procedure on the model state can be synthesized in Fig. 5, which shows the TCWV background field and the corresponding increments for the 2A12 and PATER experiments. This figure indicates that in both cases positive increments reaching 5 kg m^{-2} (negative increments down to -10 kg m^{-2}) are needed to increase (decrease) the background surface rainfall rates towards the observed values. The larger positive increments needed with 2A12 are consistent with the higher observed rainfall rates that are retrieved with this algorithm at the centre of the storm (see Fig. 3).

4.1.2 1D-Var on TMI brightness temperatures

Other 1D-Var retrievals were obtained with the minimization directly performed on the TMI brightness temperatures at 10, 19, 22 and 37 GHz in vertical polarization (V) and at 10, 19 and 37 GHz in horizontal polarization (H). Figure 6 displays the corresponding retrieved surface rainfall rates. Increasing the number of microwave channels used in the 1D-Var retrieval is expected to be beneficial especially because of their complementary sensitivity to temperature, water vapour, cloud water and precipitation. For instance, the use of the 10 GHz TBs that are particularly sensitive to the rain content avoids the saturation of the signal (i.e. the weak sensitivities) that occurs in other channels in heavy rain regions. However, adding channels also implies that more constraints are imposed during the minimization, which may hamper convergence if the relation between the brightness temperatures and the model control variable becomes strongly nonlinear. The occurrences of non-convergence can be reduced by not using the 37 GHz channels when the depolarization of observed and simulated TBs does not exceed a specified fraction of the simulated clear-sky depolarization. It was found that setting this fraction to 15% reduces the number of cases of non-convergence by 40%. Note that the 85 GHz channels have been discarded for the time being due to their strong sensitivity to ice for which the radiative transfer calculations may not be as accurate as for the liquid phase. Figure 6 illustrates the fact that 1D/TB is able to generate temperature and specific humidity increments that lead to a substantial improvement on the simulated surface rainfall rates with respect to the rainfall observations in Fig. 3.b and d. The discrepancies between observed and analysed rainfall rates are larger with the TB approach than with the method based on rainfall retrievals. This is due to the fact that the temperature and specific humidity increments result from simultaneous corrections applied to the rain profiles but also to the profiles of cloud water. Preliminary tests with less channels showed that adding the 10 GHz and 37 GHz channels leads to a slight increase of the surface rainfall rates inside the storm and to a further decrease in its vicinity. The minimization only fails to converge at a few points and in the northwest periphery of the super-typhoon's core. There, the departures between simulated and observed TBs reach such high values that the minimization problem becomes highly nonlinear so that no reasonable analysis increments can lead to the expected decrease of the simulated surface rainfall rates.

Figure 7 shows the vertical profiles of temperature and specific humidity increments produced by 1D/TB. In terms of shape, they look rather similar to the profiles obtained with 1D/RR in Fig. 4. However, as far as their magnitude is concerned, temperature increments tend to be smaller with the TB approach and the maximum increment at level 50 (around 850 hPa) that was seen in Fig. 4 (left panels) is not present in Fig. 7 (left panels). On the other hand, the specific humidity increments again dominate and are about twice as high when TBs are used in the minimization instead of surface rain rates.

Figure 8 displays maps of the TCWV increments obtained from 1D/TB. Their spatial distribution looks very similar to the one shown in Fig. 5 for 1D/RR, with positive TCWV corrections in the core of the storm, and negative values around it. It is reassuring that two very different 1D-Var methods can lead to consistent increment patterns. However, their magnitude is much stronger with absolute values exceeding 20 kg m^{-2} locally. As already mentioned, these larger TCWV increments can be explained by the fact that when working with TBs it is not only the amount of rain that is corrected, but also the amounts of water vapour and cloud water. The spotty increments to the south of the storm are due to the fact that observed TBs are interpolated onto the

model grid using the closest point approach.

4.2 Tropical cyclone Zoe

In the case of Zoe, Figure 9 shows that 1D/RR increments improve the surface rainfall rates with respect to the PATER retrieval. However, and contrary to the case of Mitag for which an almost perfect match to the observations was achieved, the improvement is mainly visible in the core of Zoe, while the rainfall amounts in the spiralling rainbands in the western and southern periphery are not reduced enough. Even in the central part of the storm, the analysed rainfall amounts are still lower than the observed values.

Comparison of the hatched areas in Fig. 3.a and Fig. 9.a shows that for Mitag most of the simulated precipitation is fully resolved by the model (large-scale ascent), while in case of Zoe, it mainly originates from the convection scheme (subgrid scale processes). The fact that the convective parameterization is still more likely to suffer from nonlinearities than the large-scale condensation scheme explains the less successful performance of 1D/RR in the case of Zoe.

With 1D/TB the analysed rainfall rates (Fig. 10) exhibit strong modifications compared to the background. Although observed surface rainfall rates are not directly involved in 1D/TB minimization, the overall improvement on this field looks more convincing than with 1D/RR. The shape of the cyclone and of the northern rainband in the analysis agree very well with the PATER retrieval (Fig. 9). The intensity of the rainfall rates reaches values larger then 10 mm h^{-1} that correspond to positive TCWV increments of up to 10 kg m^{-2} locally (not shown). TCWV increments are again much stronger and more widespread with 1D/TB than with 1D/RR (not shown). In contrast with the case of 1D/RR, the performance of 1D/TB is not much affected by the fact that convection dominates in the background. Nonlinearities in the convection scheme are indeed less detrimental in 1D/TB than in 1D/RR, because TBs are influenced by the full vertical profiles of cloud water and precipitation and are also directly related to specific humidity, beside any explicit link via the moist physics.

4.3 A mid-latitude front

Figure 11 shows the 1D/RR results for the mid-latitude front with the following layout: panel (a) displays the background surface rainfall rates, while panels (b), (d) and (f) correspond to the retrievals from PATER, Bauer-Schluessel and Ferraro. Panels (c), (e) and (g) depict the respective 1D-Var retrieved surface rainfall rates. The model's background rainfall rates are systematically higher than the three consistent SSM/I observations. However, the geographical location and structure of the simulated frontal rainband matches the observations rather well. These characteristics are very similar to the general behaviour of the ECMWF forecasting system (Chevallier and Bauer 2003) that uses more elaborate moist physical parameterizations. Again, the 1D-Var method is able to correct the temperature and specific humidity increments so that the 1D-Var retrieved surface rainfall rates match almost perfectly the available SSM/I observations. Panels (b), (d) and (f) show that significant differences are found between the rain fields retrieved with PATER-SSMI, Bauer-Schluessel and Ferraro, which is one of the major limitations of 1D/RR. The vertical profiles of temperature and specific humidity increments (not shown) exhibit a shape comparable to the one that was found for super-typhoon Mitag, but their amplitude is substantially lower due to the smaller surface rainfall departures between background and observations. Since the background field tends to overestimate the surface precipitation almost systematically over the domain, Fig. 12 shows that negative 1D-Var TCWV increments dominate, with extreme values reaching -5 kg m^{-2} locally. The values and horizontal structure of the increments look very comparable with all three retrieval algorithms.

Figure 13 displays the analysed surface rainfall rates for the mid-latitude front with 1D/TB using SSM/I observations. The main change with respect to the background field shown in Fig. 11.a is the reduction of the intensity in the southern part of the frontal rainband (below 40°N) and the slight reshaping of the front. These modifications in the analysis surface rainfall rates are also present in Fig. 14 that shows positive 1D-Var TCWV increments in the western part of the rainband that locally exceed 4 kg m^{-2}, with negative increments over the rest of the domain. The analysed rainfall rates agree fairly well with all three rainfall rates retrievals and in particular with the Ferraro algorithm (Fig. 11.e). It should be mentioned that the unchanged light rainfall values in the wake of the front correspond to grid points that were not treated in 1D/TB to save computational time (minimum threshold of 0.3 mm h^{-1} in the background).

5 Evaluation

It was shown that 1D/RR and 1D/TB lead to consistent results both in terms of analysed rainfall rates and TCWV increments. This section deals with the evaluation of the two methods based on SSM/I and TRMM data that are the only reliable observations available in precipitation areas over ocean. First, the two methods are statistically compared in TB and RR space. Then, the consistency of the vertical profiles of analysed rainfall rates is assessed using measurements from TRMM/PR for tropical cyclones Mitag and Zoe. Finally, an assessment of the impact of the observation error statistics on the 1D/TB retrievals is presented.

5.1 Evaluation in TB and RR space

For each of the three meteorological cases, brightness temperatures have been computed from the background fields and from the analyses given by the two methods, using the RTM described in section 2.2.3. The biases and the standard deviations of background-observation and analysis-observation departures are shown in Table 2 for Mitag, Zoe and the mid-latitude front and for each available microwave frequency. Statistics refer to the common points where both methods successfully converged. In all histograms the standard deviation of the analysis departures both for 1D/TB and 1D/RR is reduced with respect to the background departures. The reduction is always three to four times larger with 1D/TB than with 1D/RR for all channels. This is due to the fact that TBs are directly involved in the cost function of 1D/TB.

The biases of 1D/RR and 1D/TB analyses are generally reduced when compared to the background. The amount depends on the meteorological case and microwave channel. In the Mitag case, the bias of the background departure is small compared to the other cases, with values lower than 5 K except at 37 GHz. The two analyses and the background exhibit similar biases, except at 37 GHz where a noticeable decrease is found. In fact, the larger negative biases of background-departures for the 37 GHz channels are an artefact of the saturation of the microwave signal in the rainy core of the storm that implies the absence of offsetting large positive biases, as is the case in the other channels.

In the mid-latitude case the bias of the background departures shows large negative values, which corresponds to the presence of an excessive amount of precipitation and cloud liquid water in the background with respect to the observations. Zoe exhibits opposite features with large positive background biases of up to 15 K at several frequencies. For both cases, 1D/TB analysis biases are reduced and do not exceed a few K. A significant reduction of the bias is found with 1D/RR in the frontal case, but only a minor one in the case of Zoe. In the latter, the bias and the standard deviation of the surface rainfall analysis departures remain large, which indicates a poor convergence during the minimization. For Mitag and the mid-latitude case, largely dominated by the large-scale condensation scheme, an almost perfect agreement is found between observed and analysed

surface rainfall rates.

The smaller errors of the TB analysis departures with 1D/TB compared to 1D/RR do not necessarily correspond to smaller differences in terms of surface rainfall rates, especially for Mitag. This is due to the ambiguous link that exists between surface rainfall rates and TBs that integrate information on the whole atmospheric column. The uncertainty on the surface rainfall rates obtained with the 2A12, PATER, Bauer-Schluessel or Ferraro algorithms can also provide an explanation.

5.2 Comparison with TRMM/PR rainfall rates

Vertical profiles of rainfall rates (2A25 product; Iguchi *et al.* 2000) measured by the PR on board the TRMM platform have been used to validate the analysed rainfall rates profiles from 1D/RR and 1D/TB. The initial 2A25 product with a horizontal/vertical resolution of 1.4 km/250 m has been averaged to the model grid resolution (about 40 km/60 levels). Figure 15 shows the mean vertical profiles of rainfall rates for Mitag and Zoe. In both cases, the shape of the rain profile as observed from the PR is characterized by nearly constant values on the vertical below 600 hPa. In contrast, the mean analysed rain flux for Mitag increases from 1.5 mm h^{-1} at 600 hPa to 2.5 mm h^{-1} (resp. 4.0) at 900 hPa with 1D/RR (resp. 1D/TB). This particular shape is due to the fact that the large-scale condensation scheme is dominant in this case (see Fig. 3.a) and that it produces precipitation at all vertical levels. On the other hand, for cyclone Zoe (see Fig. 9.a), the convective scheme is more active and precipitation generation mainly occurs above 600 hPa, with a nearly constant rainfall profile below this level, as in the PR observations. The shape of the analysed rain profile seems to depend on which moist physical parameterization is the most active in the background. It should be noted that the partitioning between convective and large-scale precipitation remains comparable in the 1D-Var retrieval and in the background.

The biases and the standard deviations of the observation-analysis departures shown in Table 2 indicate that 1D/RR performs better for Mitag than for Zoe. This better behaviour in the Mitag case is also seen in Fig. 15.a. For the 1D/RR retrieval, which optimizes the surface rainfall rates, the analysed precipitation flux closely matches the radar observations below 800 hPa. In the 1D/TB method, the analysed precipitation profile is computed so as to optimize the TBs, which are mainly related to the integrated rain content and not to the surface rainfall. Hence a strong tilt of the analysed rain profile can be seen in Fig. 15.a. This is required to ensure a good agreement between the simulated and observed integrated rain contents. In the case of Zoe, the analysed rain profiles from 1D/RR and 1D/TB are closer to the radar observations than the background. However, the 1D/TB retrieval better matches the radar observations than 1D/RR, which is consistent with the results of the comparison with PATER surface rainfall rates shown in Fig. 9 and Fig. 10 and with observed TBs (Table 2).

5.3 Sensitivity to observation error statistics

In order to assess the impact of the uncertainties on the definition of the **R** matrix, some tests have been run with 1D/TB including error correlations between the TMI channels or larger standard deviations of observation errors.

Since inter-channel error correlations cannot be accurately known, two values of 0.5 and 0.8 that are representative of a low and a high level of correlation, respectively, have been tested. The corresponding biases and standard deviations of the departures between background or 1D-Var retrieval and observations as well as statistics of integrated cloud and rain water are summarized in Table 3 and Table 4 for Mitag and Zoe, respectively. Statistics have been computed over the points where the convergence was successful. As expected, the inclusion of inter-channel error correlations brings the 1D-Var retrievals closer to the background, but this

impact appears marginal.

Table 3 and Table 4 also show statistics obtained when the standard deviations of the observation errors are doubled. Again the impact on the quality of the 1D-Var results remains weak.

Therefore, it appears that the 1D-Var retrievals are not very sensitive to the specification of matrix **R**. This can be explained by the fact that because of the rather large errors specified in the current **B** matrix, the contribution of the background term, J_b, in the total cost function (Eq. (1)) is usually very small. This was confirmed by some experiments in which J_b was set to zero. Although J_b does not currently play a significant rôle in the 1D-Var retrievals, future improvements of the forecasting system will increase its contribution in J to some extent. Similar results were obtained with 1D/RR.

6 Conclusions

In this study, 1D-Var retrieval experiments based on retrieved surface rainfall rates as observed from TMI or SSM/I have been compared to 1D-Var retrieval experiments directly performed on the microwave TBs, for two tropical cyclones and an extratropical front. 1D/RR and 1D/TB include new simplified parameterizations of moist processes that perform similarly to the parameterizations used in the operational forecast model for the simulation of cloud and precipitating systems, as can be seen from comparing the results presented here to the ones documented in Chevallier and Bauer (2003).

Both 1D-Var methods produce consistent temperature and specific humidity increments that correct either the model's surface rainfall rates or the simulated TBs towards equivalent TMI or SSM/I observations. However, 1D/RR performs better when large-scale precipitation dominates in the background, due to the stronger nonlinearities that sometimes exist in convective conditions. 1D/TB seems less affected by the nature of precipitation in the background. In other respects, the 1D-Var retrievals are not very sensitive to the definition of the observation error statistics, both in terms of standard deviations and error correlations. This can be explained by the current weak contribution of the background term in the cost function.

To summarize the respective advantages and drawbacks of the two 1D-Var methods, 1D/RR (including the surface rainfall rate retrieval) has the main advantage of being computationally cheaper than 1D/TB (that requires substantial additional time for the radiative transfer calculations). The two major drawbacks of 1D/RR lie in its inefficiency wherever the background rainfall rate is zero and in its dependence on the performance of the selected rainfall algorithm. On the other hand, the fact that microwave TBs are sensitive not only to precipitation but also to water vapour and cloud water makes it possible to correct the model's control variables outside and inside rainy areas of the background in a consistent manner. 1D/TB also offers the possibility of selecting which channels should be assimilated according to the meteorological conditions (*e.g.* clear or cloudy sky, light or heavy precipitation). This flexibility also applies if one considers the changing availability of individual channels during the lifetime of a given instrument. One limitation of both 1D/RR and 1D/TB is their current inapplicability over land due to the difficulty of dealing with heterogeneities in surface emissivity. Furthermore, due to the lack of high-accuracy precipitation measurements over ocean (except maybe for the TRMM/PR), 1D-Var retrieval errors cannot be properly estimated.

An important issue that will deserve some attention in the future relates to the biases of the forward model (moist physics and/or radiative transfer), which may depend on the meteorological situation and which are not dealt with at the moment in the 1D-Var retrievals.

Since neither of the two 1D-Var methods clearly outperforms the other, their respective potential for the future operational assimilation of precipitation at ECMWF are currently under investigation in '1D-Var + 4D-Var' experiments (Marécal and Mahfouf 2002) in which pseudo-observations of TCWV produced by 1D/RR or

1D/TB on TMI and SSM/I data are assimilated in the ECMWF forecasting system. Taking advantage of the dynamical coherence of 4D-Var, these experiments will also allow the consistency of the 1D-Var retrievals with all other observations to be checked.

Acknowledgements

We would like to thank Virginie Marécal and Jean-François Mahfouf for their pioneering work on precipitation assimilation at ECMWF and for their kind support. We are grateful to INRIA (Institut National de Recherche en Informatique et en Automatique) for providing the M1QN3 mimization code. This study was supported by the European Space Agency projects EuroTRMM-2 (#12651/97/NL/NB) and EGPM (#3-10600/02/NL/GS).

References

Bauer, P. (2002). Microwave radiative transfer modelling in clouds and precipitation. Part I: Model description. Technical report. Satellite Application Facility for Numerical Weather Prediction, NWPSAF-EC-TR-005, version 1.0.

Bauer, P., Amayenc, P., Kummerow, C. D., and Smith, E. A. (2001). Over-ocean rainfall retrieval from multisensor data of the Tropical Rainfall Measuring Mission (TRMM). Part II: Algorithm implementation. *J. Ocean. Atmos. Tech.*, 18:1838–1855.

Bauer, P., Mahfouf, J.-F., Olson, W. S., Marzano, F. S., Michele, S. D., Tassa, A., and Mugnai, A. (2002). Error analysis of TMI rainfall estimates over ocean for variational data assimilation. *Q. J. R. Meteorol. Soc.*, 128:2129–2144.

Bauer, P. and Schluessel, P. (1993). Rainfall, total water, ice water, and water vapor over sea from polarized microwave simulations and special sensor microwave/imager data. *J. Geophys. Res.*, 98:20737–20759.

Chevallier, F. and Bauer, P. (2003). Model rain and clouds over oceans: comparison with SSM/I observations. *Mon. Weather Rev.*, 131:1240–1255.

Courtier, P., Thépaut, J.-N., and Hollingsworth, A. (1994). A strategy for operational implementation of 4D-Var using an incremental approach. *Q. J. R. Meteorol. Soc.*, 120:1367–1388.

Eyre, J. R. (1991). A fast radiative transfer model for satellite sounding systems. Technical report. ECMWF Technical Memorandum No. 176.

Ferraro, R. R., Weng, F., Grody, N. C., and Basist, A. (1996). An eight-year (1987-1994) time series of rainfall, clouds, water vapor, snow cover, and sea ice derived from SSMI measurements. *Bull. Am. Meteorol. Soc.*, 77:891–905.

Fillion, J.-L. and Mahfouf, J.-F. (2000). Coupling of moist-convective and stratiform precipitation processes for variational data assimilation. *Mon. Weather Rev.*, 128:109–124.

Gilbert, J.-C. and Lemaréchal, C. (1989). Some numerical experiments with variable-storage quasi-Newton algorithms. *Math. Programming*, 45:407–435.

Holtslag, A. A. M. and Moeng, C.-H. (1991). Eddy diffusivity and countergradient transport in the convective atmospheric boundary layer. *J. Atmos. Sci.*, 48:1690–1698.

Iguchi, T., Meneghini, R., Awaka, J., Kozu, T., and Okamoto, K. (2000). Rain profiling algorithm for TRMM precipitation radar data. *Advances in Space Research, Oxford, England*, 25:973–976.

Janisková, M., Mahfouf, J.-F., Morcrette, J.-J., and Chevallier, F. (2002). Linearized radiation and cloud schemes in the ECMWF model: Development and evaluation. *Q. J. R. Meteorol. Soc.*, 128:1505–1527.

Kummerow, C. D. (1993). On the accuracy of the Eddington-approximation for the radiative transfer in microwave frequencies. *J. Geophys. Res.*, 98:2757–2765.

Kummerow, C. D., Hong, Y., Olson, W. S., Yang, S., Adler, R. F., McCollum, J., Ferraro, R., Petty, G., Shin, D.-B., and Wilheit, T. T. (2001). The Evolution of the Goddard Profiling Algorithm (GPROF) for Rainfall Estimation from Passive Microwave Sensors. *J. Appl. Meteor.*, 40:1801–1820.

L'Ecuyer, T. S. and Stephens, G. L. (2002). An uncertainty model for Bayesian Monte Carlo retrieval algorithms: Application to the TRMM observing system. *Q. J. R. Meteorol. Soc.*, 128:1713–1738.

Lopez, P. and Moreau, E. (2003). A convection scheme for data assimilation: Description and initial tests. Technical report. ECMWF Technical Memorandum No. 411.

Marécal, V. and Mahfouf, J.-F. (2000). Variational retrieval of temperature and humidity profiles from TRMM precipitation data. *Mon. Weather Rev.*, 128:3853–3866.

Marécal, V. and Mahfouf, J.-F. (2002). Experiments on 4D-Var assimilation of rainfall data using an incremental formulation. Technical report. In press.

Marécal, V., Mahfouf, J.-F., and Bauer, P. (2002). Comparison of TMI rainfall estimates and their impact on 4D-Var assimilation. *Q. J. R. Meteorol. Soc.*, 128:2737–2758.

Moreau, E., Bauer, P., and Chevallier, F. (2002). Microwave radiative transfer modelling in clouds and precipitation. Part II: Model evaluation. Technical report. Satellite Application Facility for Numerical Weather Prediction, NWPSAF-EC-TR-005, version 1.0.

Moreau, E., Bauer, P., and Chevallier, F. (2003). Variational retrieval of rain profiles from spaceborne passive microwave radiance observations. *J. Geophys. Res.* accepted.

Rabier, F., McNally, A., Andersson, E., Courtier, P., Unden, P., Eyre, J., Hollingsworth, A., and Bouttier, F. (1997). The ECMWF implementation of the three dimensional variational assimilation (3D-Var). Part II: Structure functions. *Q. J. R. Meteorol. Soc.*, 124:1809–1829.

Saunders, R., Brunel, P., Chevallier, F., Deblonde, G., English, S. J., Matricardi, M., and Rayer, P. (2002). RTTOV-7 science and validation report. Technical report. Met Office Forecasting and Research Technical Report No. 387.

Simpson, J. and Wiggert, V. (1969). Models of precipitating cumulus towers. *Mon. Weather Rev.*, 97:471–489.

Sundqvist, H., Berge, E., and Kristjánsson, J. E. (1989). Condensation and cloud parameterization studies with a mesoscale numerical weather prediction model. *Mon. Weather Rev.*, 117:1641–1657.

Tiedtke, M. (1989). A comprehensive mass flux scheme for cumulus parameterization in large-scale models. *Mon. Weather Rev.*, 117:1779–1800.

Tiedtke, M. (1993). Representation of clouds in large-scale models. *Mon. Weather Rev.*, 121:3040–3061.

Tompkins, A. M. and Janisková, M. (2003). A cloud scheme for data assimilation: Description and initial tests. Technical report. ECMWF Technical Memorandum No. 410.

Model level number	Pressure (hPa)
20	36
25	96
30	202
35	353
40	539
45	728
50	884
55	979
60	1012

Table 1: Pressure (in hPa) on every five model levels between levels 20 and 60. Values are given assuming a surface pressure of 1013.25 hPa.

Case	typhoon Mitag						cyclone Zoe						Front					
Experiment	Guess		1D/TB		1D/RR		Guess		1D/TB		1D/RR		Guess		1D/TB		1D/RR	
Channels (GHz)	*observation−model TB bias and standard deviation [K]*																	
10 V	−1.6	**11.4**	−2.0	**2.8**	−0.8	**7.0**	6.0	**14.0**	−1.0	**3.4**	3.0	**11.2**	–	–	–	–	–	–
19 V	0.9	**14.4**	2.0	**2.2**	4.1	**8.6**	10.6	**13.6**	1.3	**3.0**	7.8	**12.6**	−4.3	**10.6**	0.5	**2.1**	2.9	**7.5**
22 V	−0.1	**8.2**	1.1	**1.7**	2.5	**4.8**	5.7	**6.0**	1.1	**2.7**	5.0	**6.1**	−1.7	**8.3**	1.9	**2.0**	3.9	**6.4**
37 V	−5.3	**15.9**	−1.4	**4.3**	0.8	**9.6**	10.2	**12.8**	3.4	**9.4**	9.9	**13.2**	−7.7	**14.2**	−1.8	**3.2**	0.5	**10.8**
10 H	−4.7	**20.4**	−5.4	**5.0**	−3.2	**12.4**	10.1	**25.9**	−2.7	**6.5**	4.5	**20.7**	–	–	–	–	–	–
19 H	−2.1	**26.7**	−0.2	**4.4**	3.5	**16.1**	15.5	**26.1**	−1.6	**5.2**	10.0	**23.9**	−10.2	**20.5**	−1.2	**4.3**	3.6	**14.3**
37 H	−10.2	**32.1**	−2.7	**5.8**	1.7	**19.4**	16.7	**25.7**	1.0	**11.9**	14.3	**25.6**	−17.5	**30.1**	−5.2	**6.9**	1.1	**23.3**
	bias and standard deviation of PATER observations−model [mm h^{-1}]																	
Surface rainfall	−0.04	**1.58**	−0.45	**1.73**	−0.02	**0.11**	2.6	**4.6**	1.2	**3.0**	2.0	**3.5**	−0.86	**1.09**	−0.42	**0.91**	−0.02	**0.22**

Table 2: 1D-Var statistics from background and analysis for the 1D/TB and the 1D/RR experiments for the three studied cases. Biases and standard deviations of observation−background and observation−analysis departures in terms of TBs and in terms of surface rainfall rates. Standard deviations are in bold font.

Experiment	Background		No correl.		Correl.= 0.5		Correl.= 0.8		$2 \times \sigma_{obs}$	
Channel (GHz)	*observation−model TB bias and standard deviation [K]*									
10 V	−1.8	**11.6**	−2.0	**3.1**	−2.4	**3.4**	−2.8	**3.9**	−1.8	**3.7**
19 V	0.6	**14.6**	1.9	**2.4**	0.8	**3.2**	0.1	**4.1**	1.9	**2.5**
21 V	−0.2	**8.3**	1.1	**1.6**	0.1	**2.3**	−0.6	**3.0**	1.0	**1.8**
37 V	−5.4	**16.2**	−1.5	**3.8**	−2.8	**4.0**	−3.4	**4.6**	−1.9	**3.9**
10 H	−5.1	**20.7**	−5.4	**5.5**	−6.1	**6.3**	−6.7	**7.1**	−4.9	**6.6**
19 H	−2.9	**27.0**	−0.4	**4.7**	−2.4	**6.2**	−3.8	**7.5**	−0.4	**5.1**
37 H	−10.7	**32.6**	−3.0	**5.4**	−5.7	**6.1**	−7.1	**7.5**	−3.9	**6.1**
Integrated contents	*mean and standard deviation [kg m^{-2}]*									
rain water	0.22	**0.32**	0.23	**0.44**	0.24	**0.45**	0.25	**0.45**	0.22	**0.39**
cloud water	0.64	**0.63**	0.62	**0.84**	0.64	**0.84**	0.64	**0.81**	0.62	**0.82**

Table 3: Impact of the inclusion of TMI channel error correlations on the 1D-Var retrievals in the case of super-typhoon Mitag: biases and standard deviations of observation−background and observation−analysis departures for all channels used, and means and standard deviations of integrated cloud and rain water contents. Standard deviations are in bold font.

Experiment	Background		No correl.		Correl.= 0.5		Correl.= 0.8		$2 \times \sigma_{obs}$	
Channel (GHz)	*observation−model TB bias and standard deviation [K]*									
10 V	3.4	**14.6**	−1.0	**3.9**	−1.0	**4.7**	−1.1	**5.0**	−0.5	**4.4**
19 V	8.1	**14.3**	1.8	**3.1**	1.5	**3.8**	1.4	**4.5**	2.0	**3.0**
21 V	4.9	**6.4**	1.6	**2.7**	1.3	**3.0**	1.1	**3.3**	1.7	**2.4**
37 V	8.0	**13.4**	2.5	**8.4**	2.3	**9.0**	1.8	**8.8**	2.6	**8.3**
10 H	5.2	**27.2**	−2.5	**7.4**	−2.6	**8.8**	−2.7	**9.1**	−1.7	**8.3**
19 H	10.4	**27.6**	−0.4	**5.5**	−1.0	**6.4**	−1.3	**7.6**	−0.2	**5.7**
37 H	11.0	**27.7**	0.1	**9.2**	−0.6	**10.3**	−1.3	**10.9**	0.2	**9.2**
Integrated contents	*mean and standard deviation [kg m^{-2}]*									
rain water	0.44	**0.62**	0.56	**0.64**	0.58	**0.64**	0.57	**0.64**	0.54	**0.60**
cloud water	0.62	**0.51**	0.92	**0.92**	0.94	**0.91**	0.92	**0.89**	0.90	**0.90**

Table 4: Same as in Table 3, but for tropical cyclone Zoe.

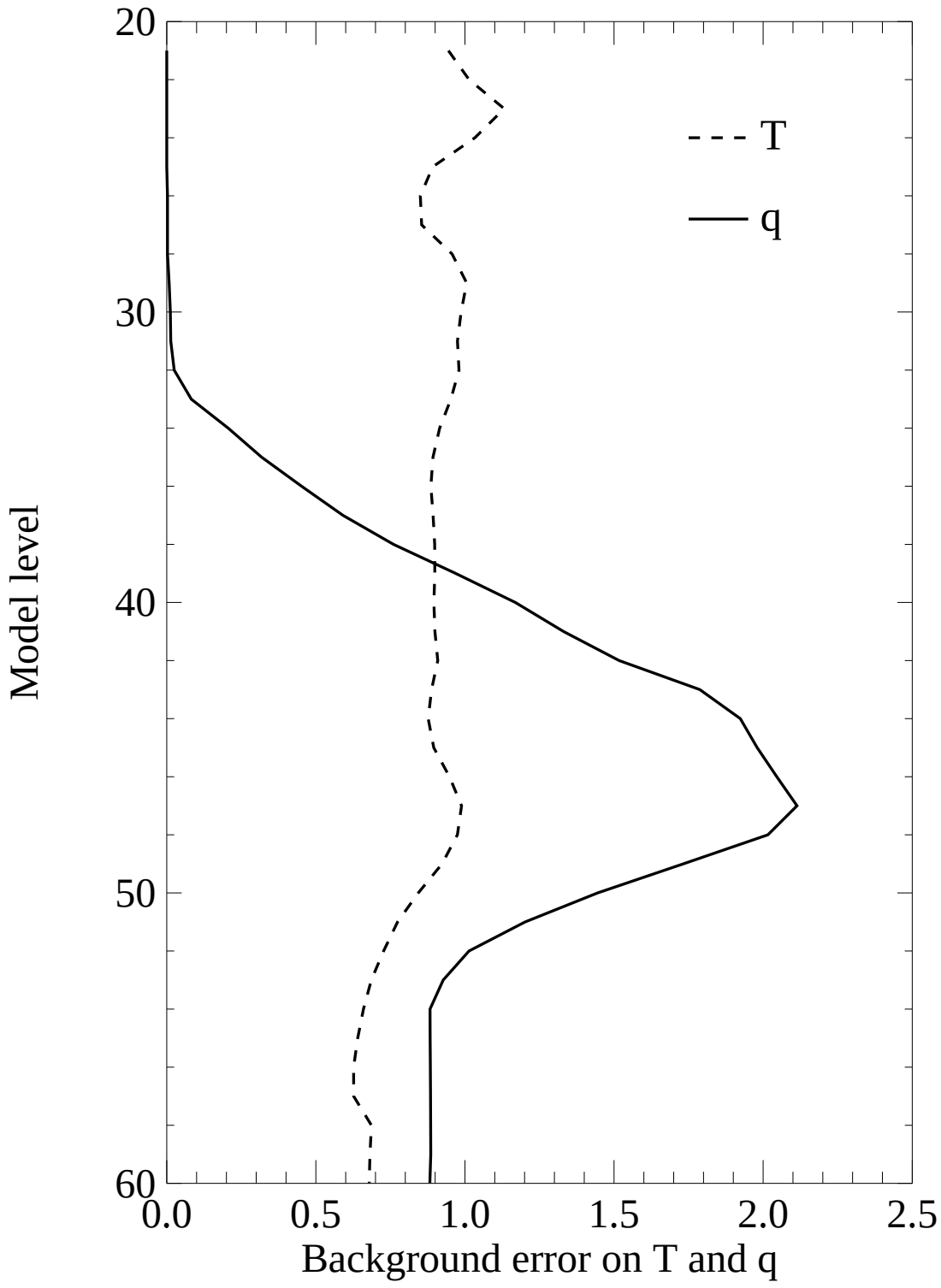

Figure 1: Vertical profiles of typical values of the standard deviation of the model background errors on temperature (dashed line) and specific humidity (solid line). Units are in K and g kg^{-1} respectively.

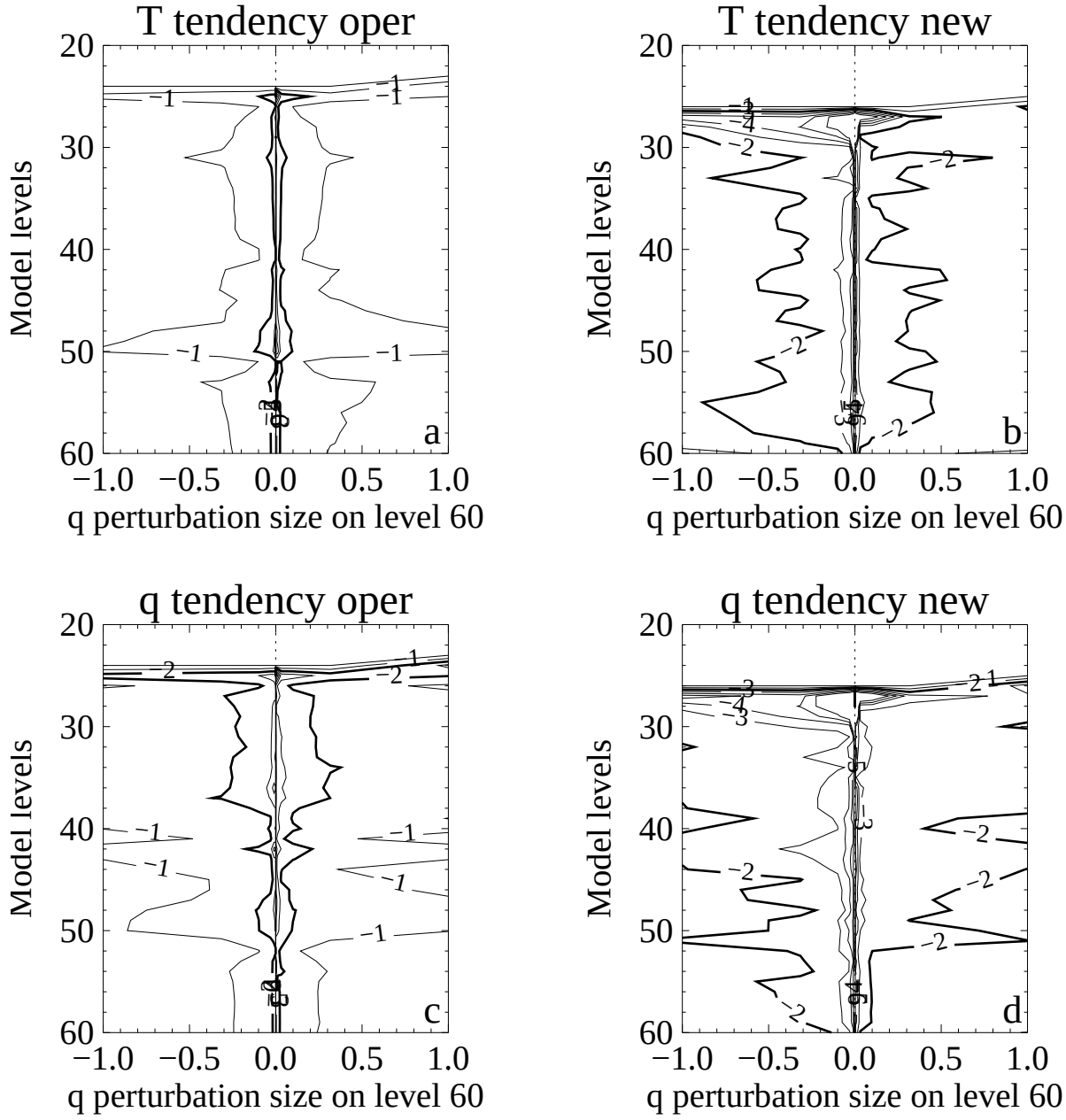

Figure 2: Nonlinear residuals of convective temperature and specific humidity tendencies as functions of parameter λ that determines the size of the input specific humidity perturbations imposed on model level 60. The displayed residuals have been averaged over one hundred convective profiles. The field actually plotted is $\log_{10}(RES_{NL}/RES_{NL}^{max})$ where RES_{NL}^{max} denotes the maximum value of the residual for a given pair of input/output parameters and for both studied convection schemes (*i.e.* for a given row of the figure). Left: operational scheme, right: new scheme.

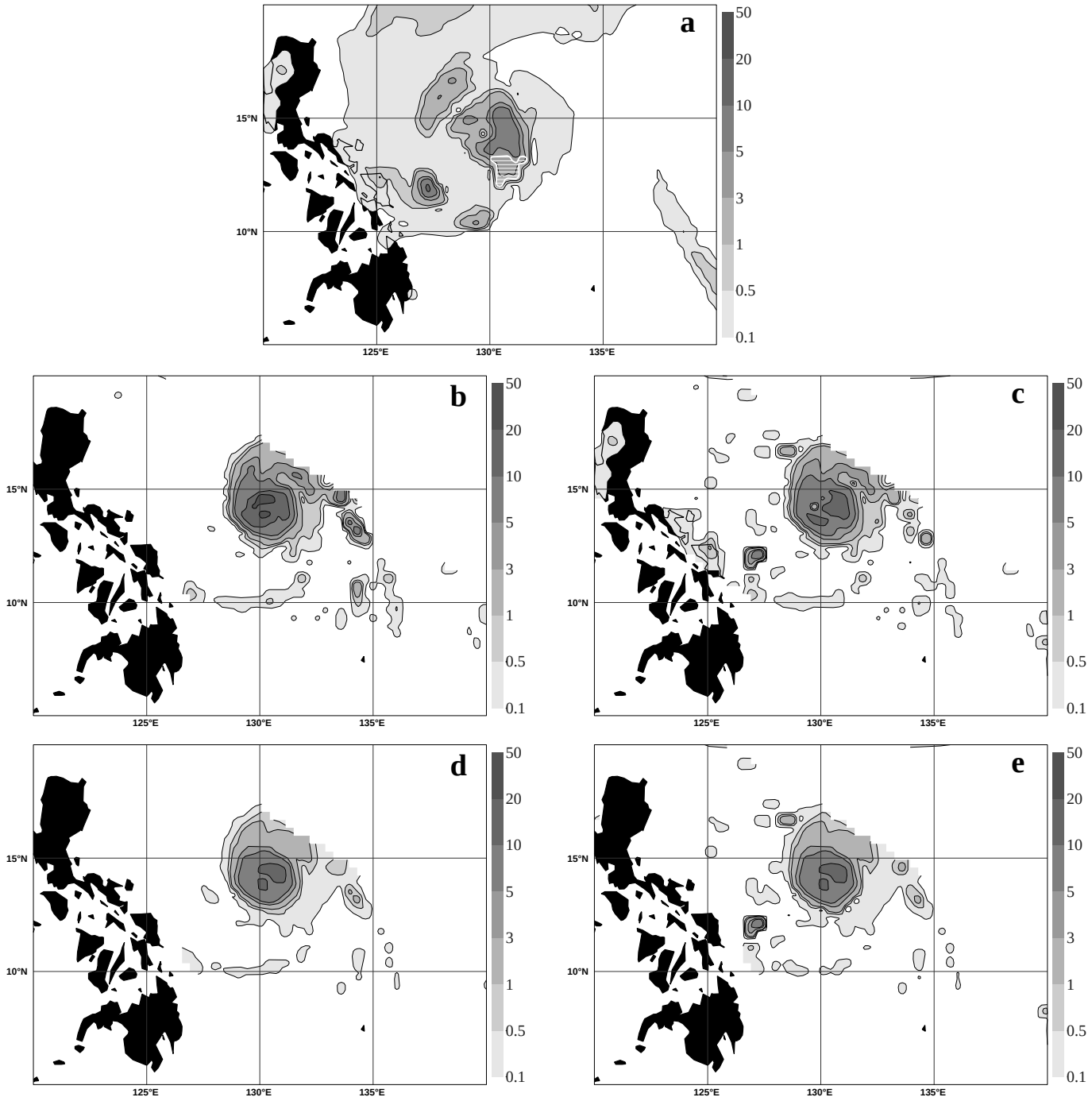

Figure 3: 1D-Var on TMI derived surface rainfall rates for the case of super-typhoon Mitag at 1200 UTC 5 March 2002: Rain rates from model background (a), 2A12 (b) and PATER (d) and as from the corresponding 1D-Var analysis (c and e respectively). Units are in mm h^{-1}. The white hatched area indicates the regions where surface convective rainfall represents more than 50% of the total surface rainfall.

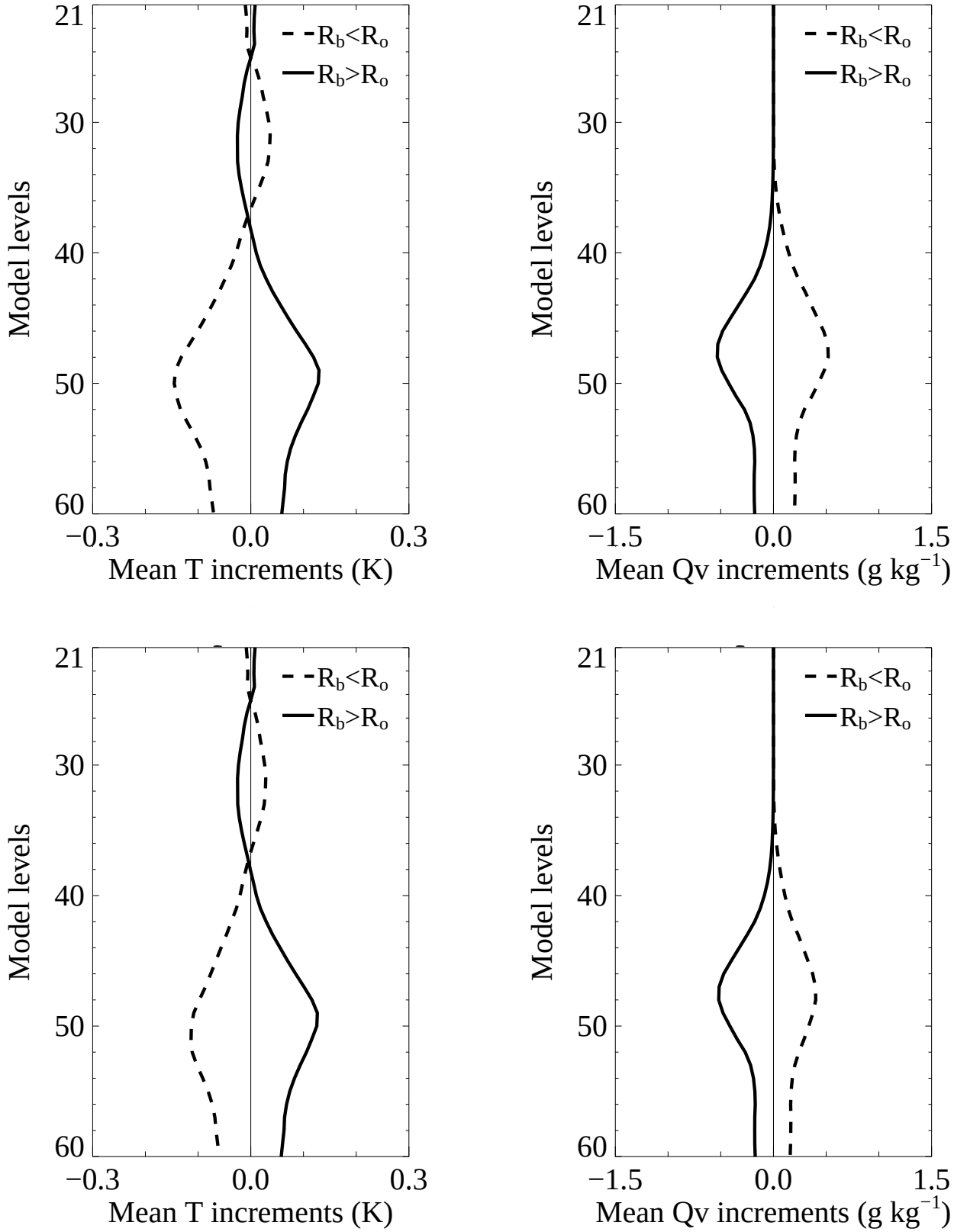

Figure 4: 1D-Var on TMI derived surface rainfall rates for the case of super-typhoon Mitag at 1200 UTC 5 March 2002: Mean vertical profiles of the increments in temperature (left panel) and specific humidity (right panel) when using rainfall observations from 2A12 (top) and from PATER (bottom). Cases for which the background rainfall rate needs to be increased (resp. decreased) are plotted with a dashed line (resp. solid line). Model level 60 is close to the surface and model level 21 roughly corresponds to 50 hPa.

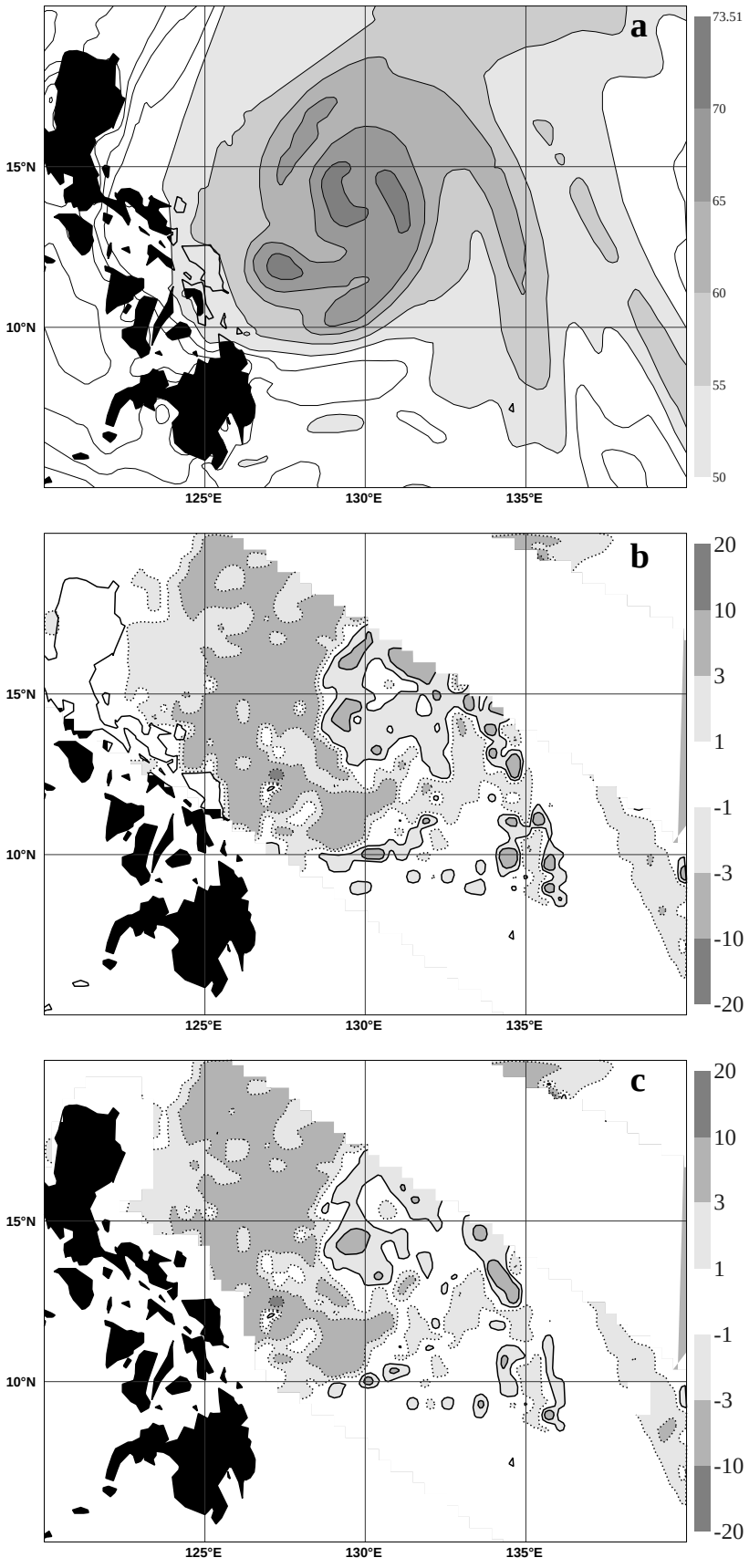

Figure 5: 1D-Var on TMI derived surface rainfall rates for the case of super-typhoon Mitag at 1200 UTC 5 March 2002: Background field of TCWV (a) and TCWV increments when using surface rainfall rates from 2A12 (b) and from PATER (c). Units are in kg m^{-2}.

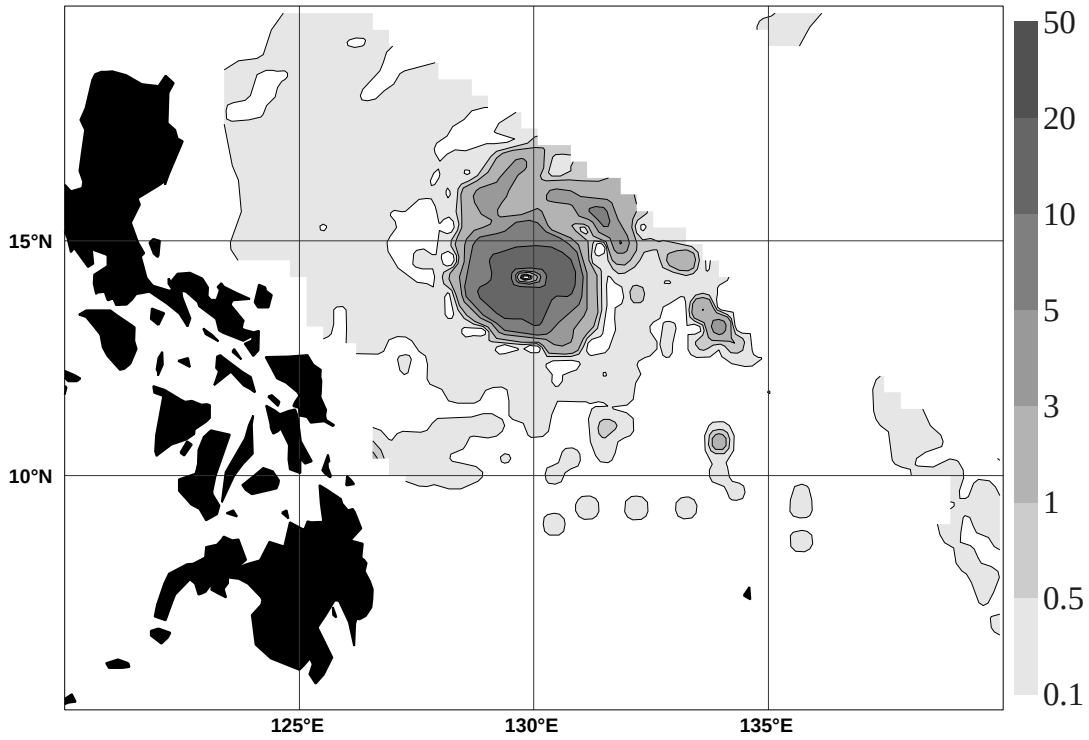

Figure 6: 1D-Var on TMI microwave brightness temperatures for the case of super-typhoon Mitag at 1200 UTC 5 March 2002: 1D-Var retrieved surface rainfall rates in mm h^{-1}.

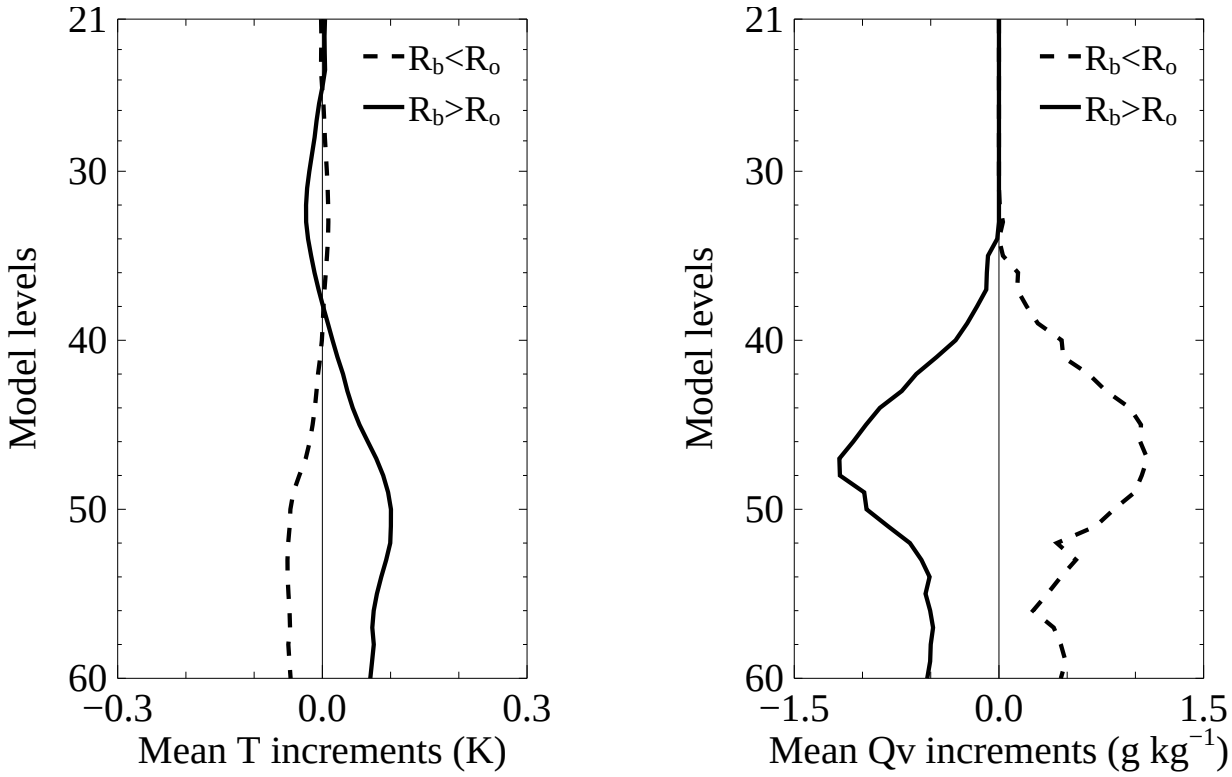

Figure 7: 1D-Var on TMI microwave brightness temperatures for the case of super-typhoon Mitag at 1200 UTC 5 March 2002: Mean vertical profiles of the increments in temperature (left panel) and specific humidity (right panel). Same plotting conventions as in Fig. 4.

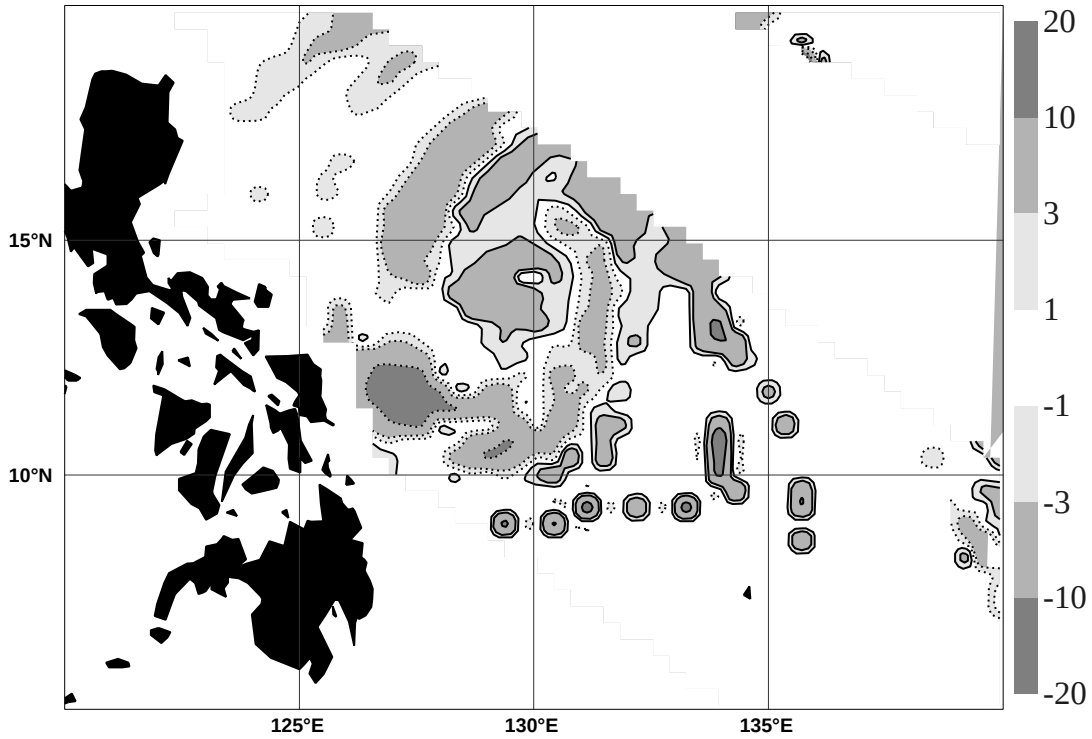

Figure 8: 1D-Var on TMI microwave brightness temperatures for the case of super-typhoon Mitag at 1200 UTC 5 March 2002: TCWV increments in kg m^{-2}.

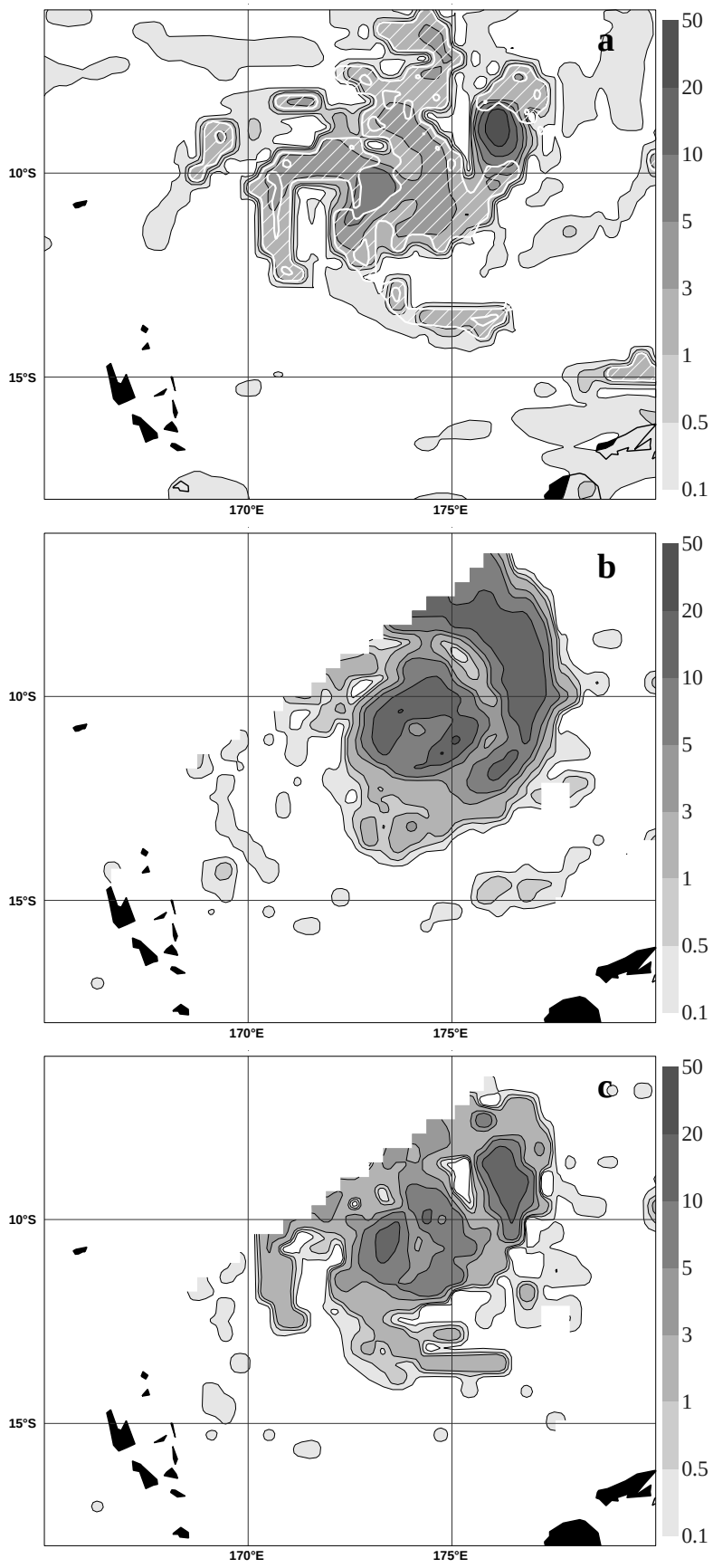

Figure 9: Same as in Fig. 3 but for the case of tropical cyclone Zoe at 1200 UTC 26 December 2002: Rain rates from model background (a), PATER (b) and as from the corresponding 1D-Var analysis (c).

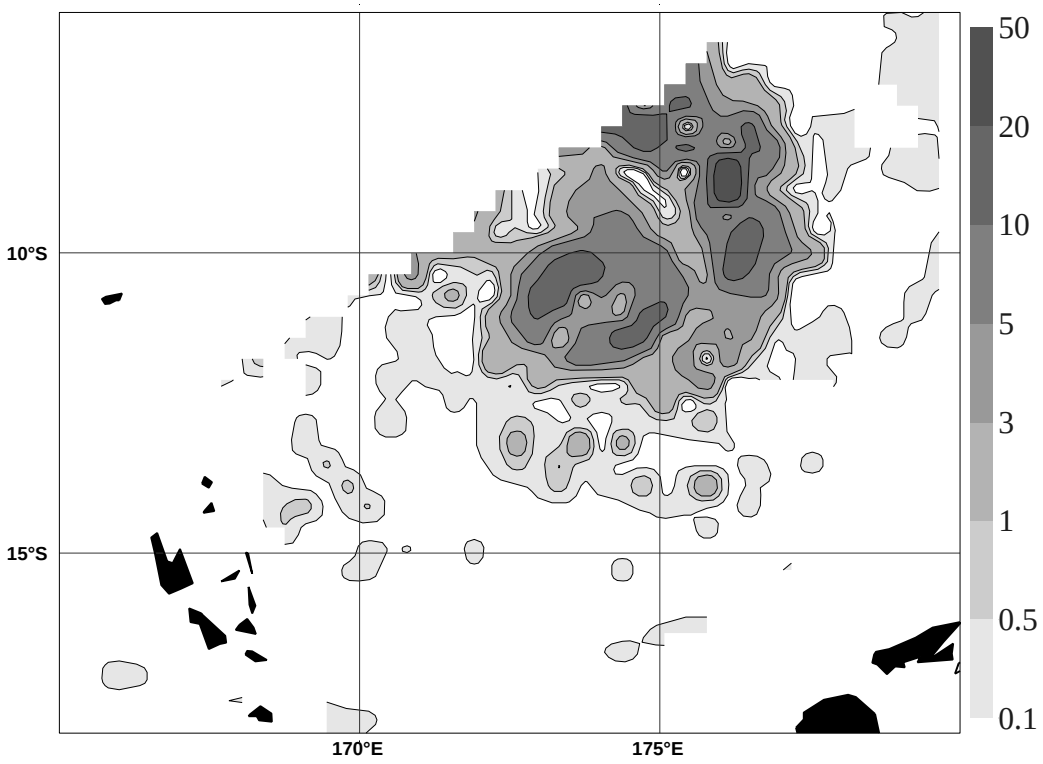

Figure 10: 1D-Var on TMI microwave brightness temperatures for the case of tropical cyclone Zoe at 1200 UTC 26 December 2002: 1D-Var retrieved surface rainfall rates in mm h^{-1}.

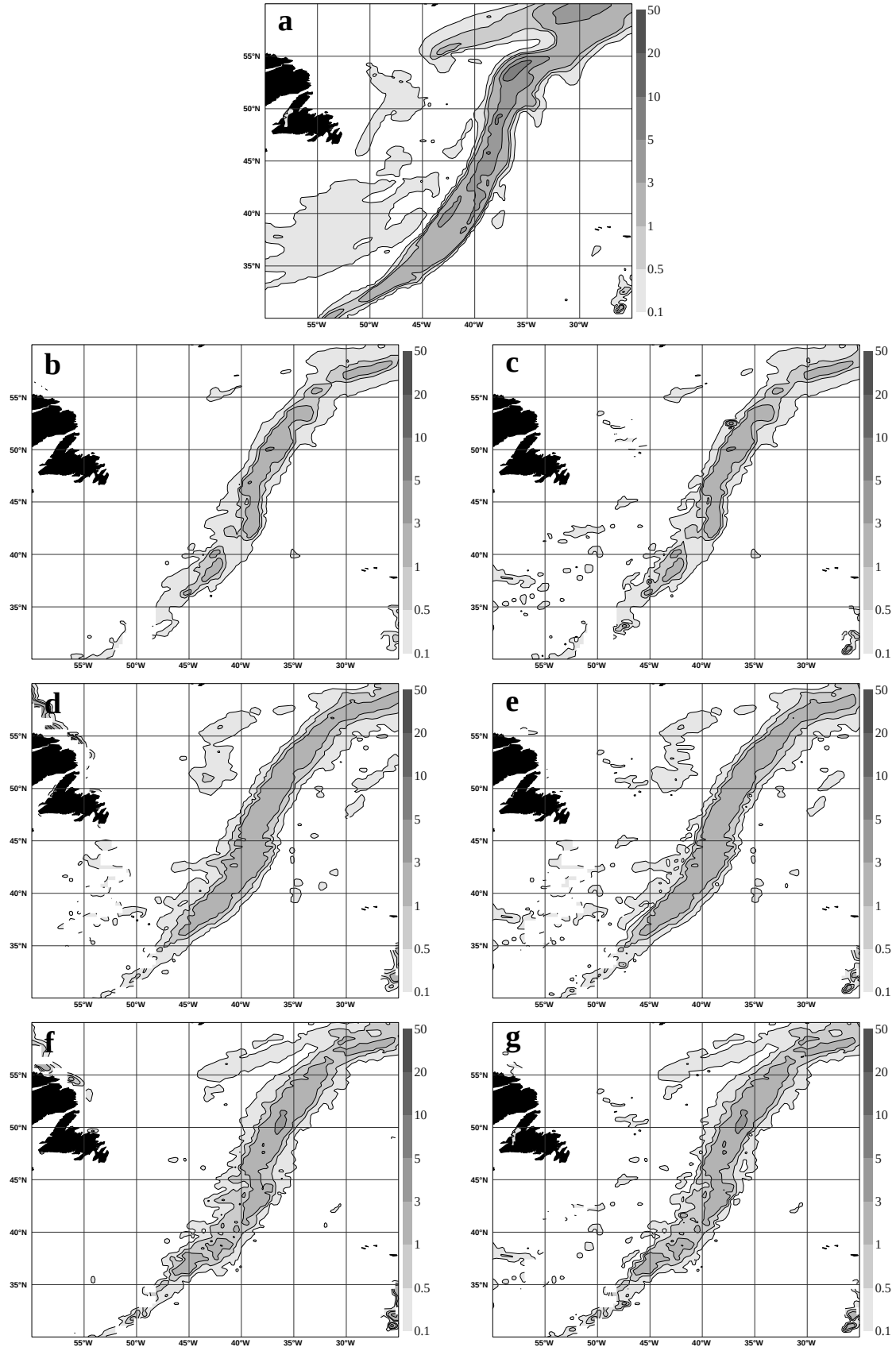

Figure 11: 1D-Var on SSM/I derived surface rainfall rates for the case of the North-Atlantic front at 1200 UTC 9 January 2002: Rain rates from model background (a), PATER (b), Bauer-Schluessel (d) and Ferraro (f) and as in the corresponding 1D-Var analysis (c, e and g, respectively). Units are in mm h^{-1}.

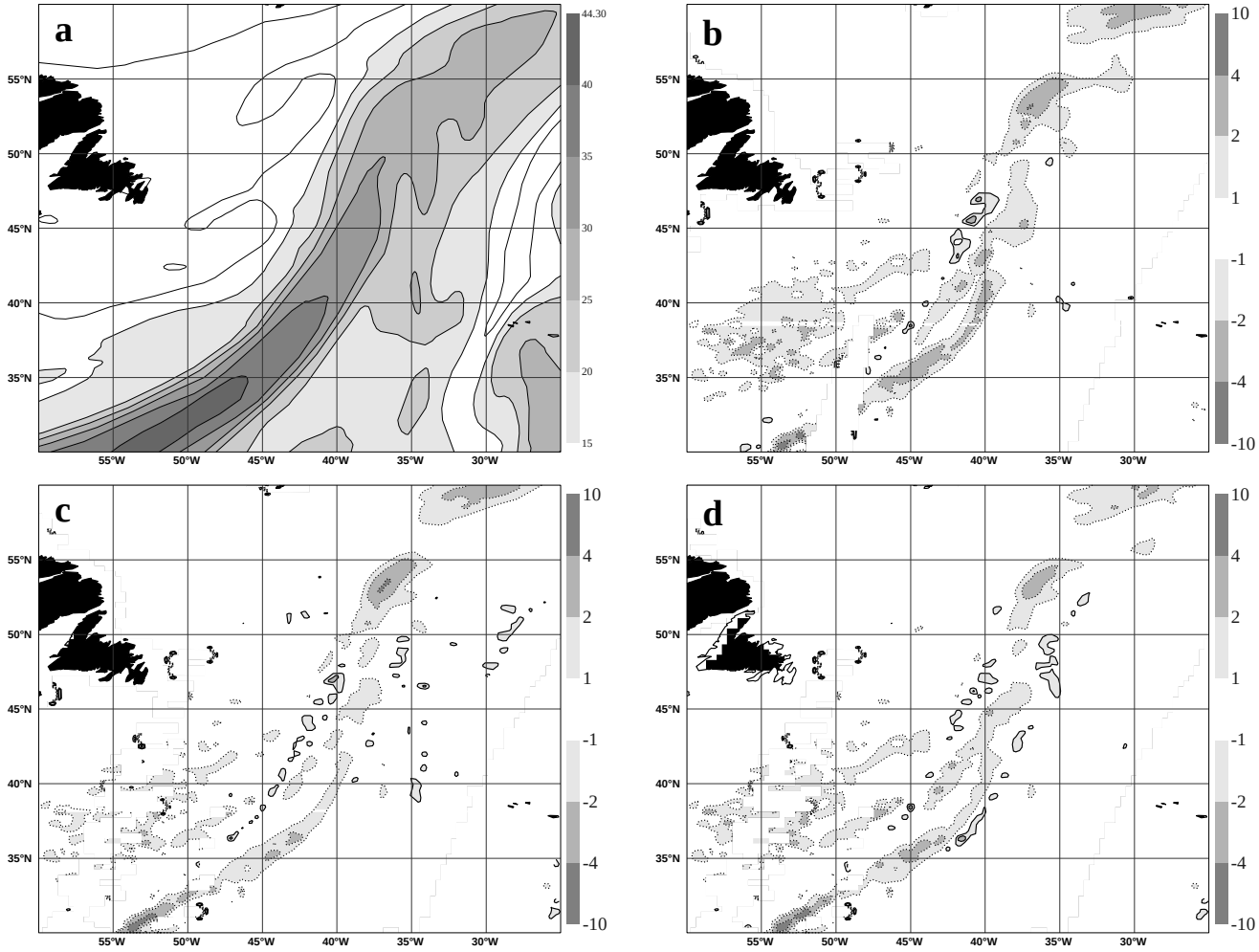

Figure 12: 1D-Var on SSM/I derived surface rainfall rates for the case of North-Atlantic front at 1200 UTC 9 January 2002: Background field of TCWV (a) and TCWV increments when using surface rainfall rates from PATER (b), Bauer-Schluessel (c) and Ferraro (d). Units are in kg m^{-2}.

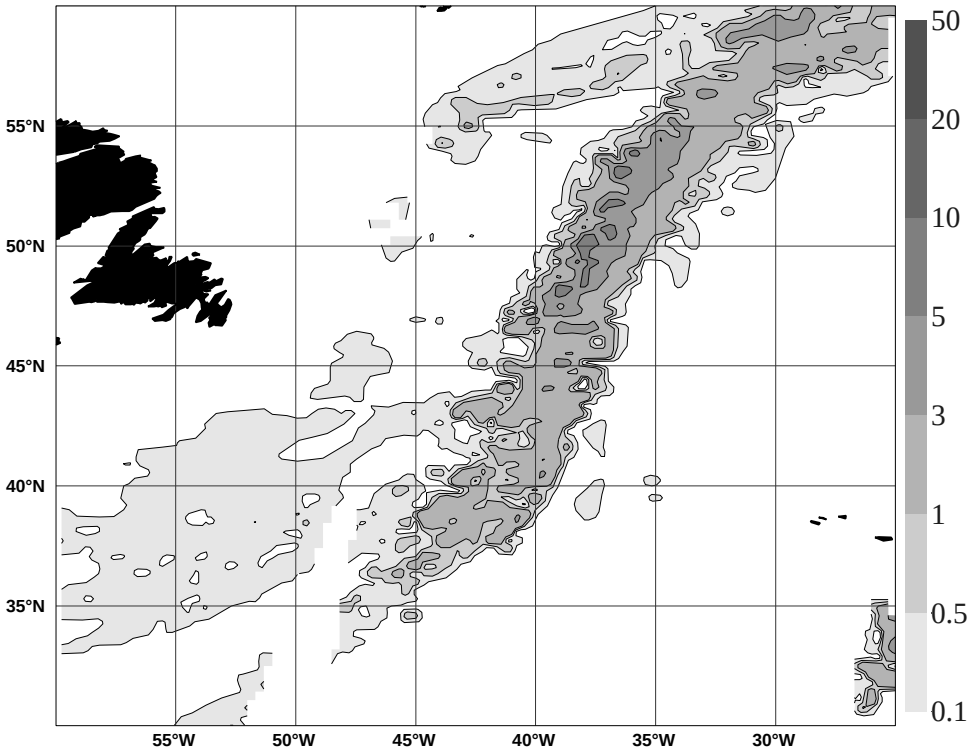

Figure 13: 1D-Var on SSM/I microwave brightness temperatures for the case of North-Atlantic front at 1200 UTC 9 January 2002: 1D-Var retrieved surface rainfall rates in mm h^{-1}.

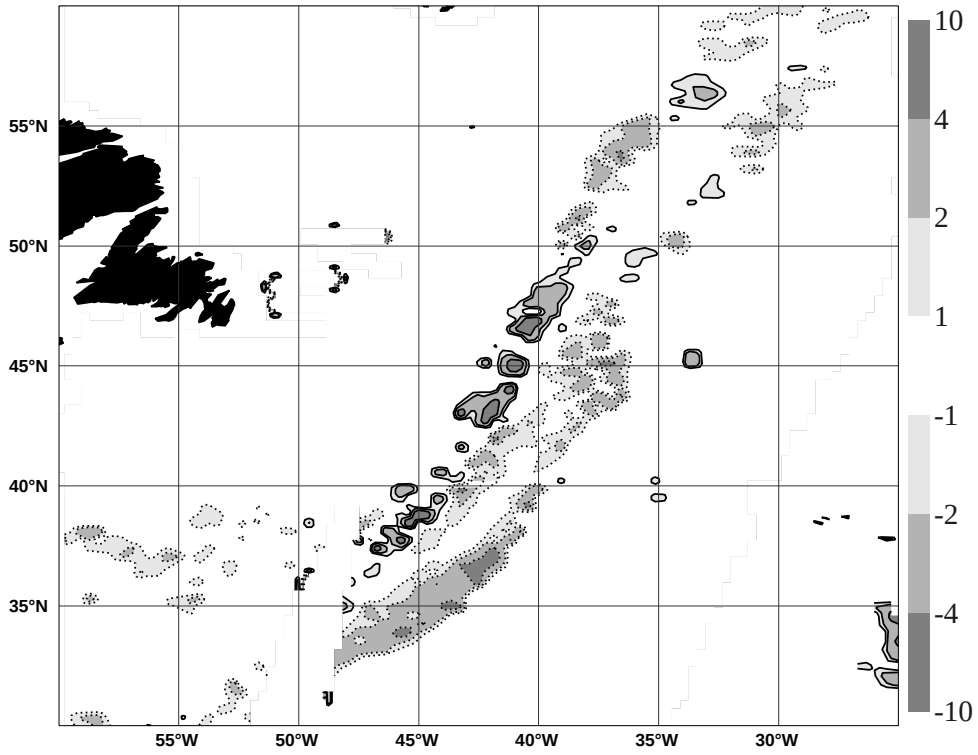

Figure 14: 1D-Var on SSM/I microwave brightness temperatures for the case of North-Atlantic front at 1200 UTC 9 January 2002: TCWV increments in kg m^{-2}.

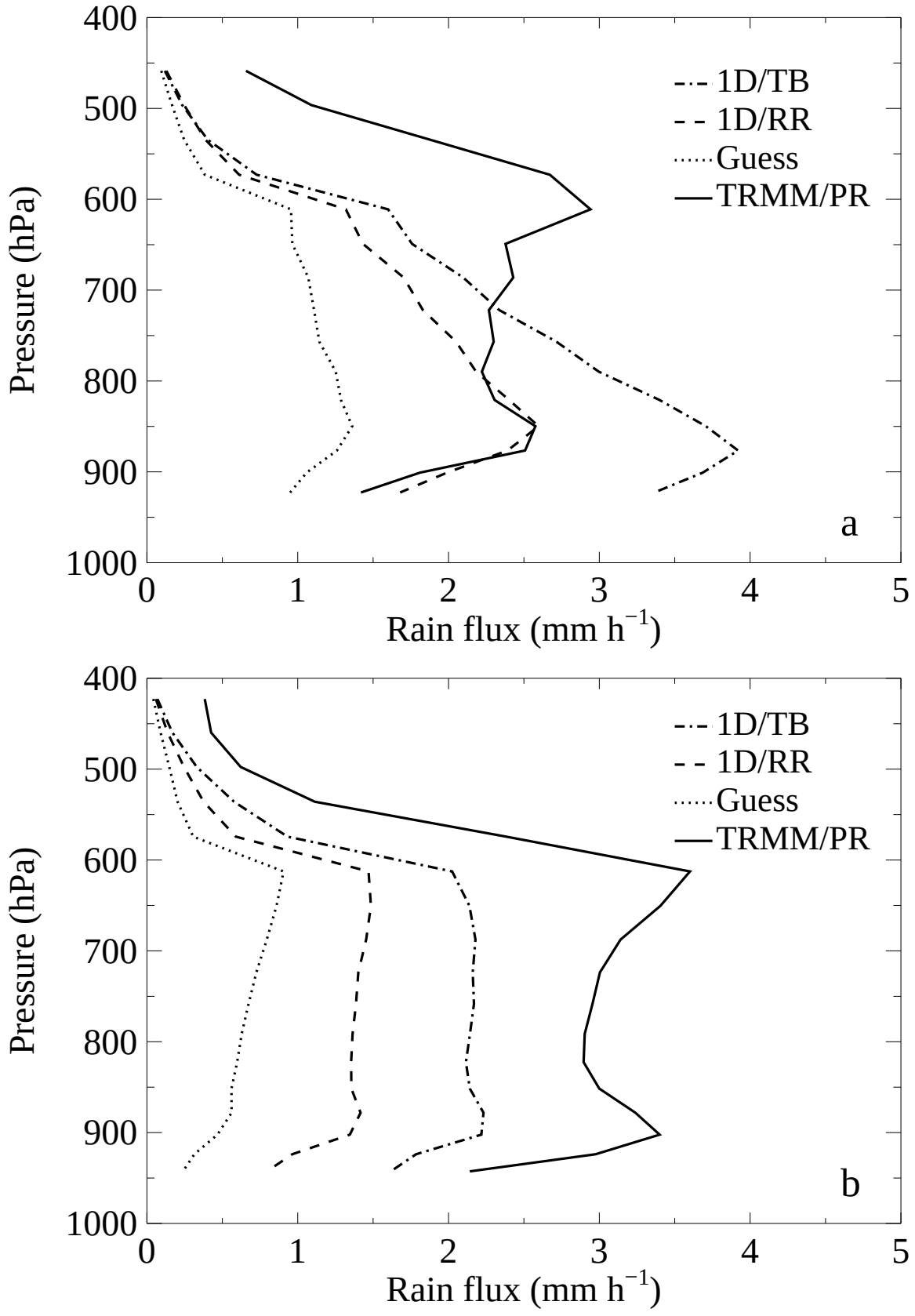

Figure 15: Horizontally averaged vertical profiles of rainfall rates from TRMM/PR observations, from the background, from 1D/RR and from 1D/TB. Results are shown for Mitag (a) and Zoe (b). Units are in mm h^{-1}.